Accumulation of styrene oligomers alters lipid membrane phase order and miscibility

Mattia I. Morandi[a,1], Monika Kluzek[a], Jean Wolff[a], André Schroder[a], Fabrice Thalmann[a], and Carlos M. Marques[a,1]

[a]Institut Charles Sadron, Université de Strasbourg, CNRS, UPR022, 67034 Strasbourg Cedex, France

Edited by David A. Weitz, Harvard University, Cambridge, MA, and approved December 20, 2020 (received for review July 31, 2020)

Growth of plastic waste in the natural environment, and in particular in the oceans, has raised the accumulation of polystyrene and other polymeric species in eukyarotic cells to the level of a credible and systemic threat. Oligomers, the smallest products of polymer degradation or incomplete polymerization reactions, are the first species to leach out of macroscopic or nanoscopic plastic materials. However, the fundamental mechanisms of interaction between oligomers and polymers with the different cell components are yet to be elucidated. Simulations performed on lipid bilayers showed changes in membrane mechanical properties induced by polystyrene, but experimental results performed on cell membranes or on cell membrane models are still missing. We focus here on understanding how embedded styrene oligomers affect the phase behavior of model membranes using a combination of scattering, fluorescence, and calorimetric techniques. Our results show that styrene oligomers disrupt the phase behavior of lipid membranes, modifying the thermodynamics of the transition through a spatial modulation of lipid composition.

nanopollution | lipid bilayer phase separation | SANS | Laurdan

The increasing amount of plastic present in sea waters has become a major issue in recent years, with increasing concerns regarding the potential hazardous effects it may have on living systems (1, 2). Annual production of plastic has reached almost 300 million tons/y, of which 5 to 13 million tons are estimated to reach the oceans by different means (3). While initially the main concern for plastic contamination was the presence of microplastic, produced by polymeric degradation, recently the focus has shifted to nanoplastic (4, 5). Objects of this scale can easily enter the food chain via digestion and there is increasing evidence of plastic micro- and nanoobjects found in marine life forms (6–9). Moreover, nanometer-size polymer particles are also produced industrially for specific research and technological applications, such as imaging, sensing, and preparation of nanocomposites (10), providing a second route, besides degradation, for plastic-derived nanoparticles' entry into sea waters. Despite a current lack of evidence on the presence of nanoobjects (4), studies have indeed shown that plastic nanoparticles can accumulate in the tissues of living organisms and disrupt their metabolism (11–13) and that size plays an important role in determining their accumulation (12, 13). However, a physicochemical characterization of the interaction between plastic nanoobjects and living organisms is still lacking, especially regarding the mechanisms of potential toxicity. As the first barrier encountered by any foreign object entering an organism, the cell membrane is the primary candidate of investigation in assessing possible toxicity of plastic nanofragments. In particular, the membrane lipid lateral organization plays a crucial role in many cellular signaling processes due to the presence in the membrane of small transient domains called "lipid rafts," and even minute changes in membrane lipid organization can result in a potential alteration of these processes and pose a threat to cellular viability.

Polystyrene is one of the most commonly used plastics in the world, contributing to a significant fraction of marine plastic wastes in the form of styrene oligomers (SO) (14), and it has been shown in several studies to directly affect lipid bilayer physical properties when accumulated within the membrane. Accumulation of styrene oligomers and polymers in 1-palmitoyl-2-oleoyl-*sn*-glycero-3-phosphocholine bilayers indeed showed, in numerical simulations, to change the membrane mechanical properties and lateral lipid organization (15) and a stabilization of cholesterol-induced domains (16). However, experimental studies on the effects of polystyrene and oligomers in the cell membrane and model membranes are still lacking. It was previously reported that incorporation of styrene monomers into lipid membranes significantly changes the fluidity of the membrane (17), and a similar effect was indeed shown for charged polystyrene sulfonated chains in surfactant bilayers (18), but from an experimental point of view many aspects of the interaction are still elusive. In this work we investigate the effects of styrene oligomers (M_n = 500 Da) on the phase transition of lipid bilayers composed of unsaturated lipids or a mixture of unsaturated/saturated lipids, to obtain a more comprehensive picture of the role of membrane complexity on the effects of styrene oligomer accumulation. Indeed, small styrene chains display the largest mobility; they are the most likely to be transferred to the lipid membranes upon contact with a degrading piece of plastic. Also, when one considers the important role played by the gel–liquid transition point of the saturated lipid in the formation of domains in ternary lipid mixtures relevant for biomembranes, it becomes clear that the most fundamental question to be asked in this context is that of the influence of the oligomers on the gel–liquid transition of the saturated lipid. We investigated the changes in transition using differential scanning calorimetry

Significance

Accumulation of nanopollutants in lifeforms has become the subject of increasing concern, but effects are not understood. Biological systems are inherently complex, and therefore any small variations on the membrane properties can potentially perturb cell functionality. In this study we observe that the presence of styrene oligomers in lipid membranes alters their phase behavior, with stronger changes occurring in more complex systems, which could translate into potential cellular disruption. This study provides evidence that the presence of nanopollutants in the membrane may alter its fundamental properties and affect cell viability.

Author contributions: M.I.M., M.K., F.T., and C.M.M. designed research; M.I.M., M.K., J.W., A.S., F.T., and C.M.M. performed research; M.I.M., M.K., J.W., A.S., F.T., and C.M.M. analyzed data; and M.I.M., F.T., and C.M.M. wrote the paper.

The authors declare no competing interest.

This article is a PNAS Direct Submission.

[1]To whom correspondence may be addressed. Email: marques@unistra.fr or mattia.morandi@weizmann.ac.il.

This article contains supporting information online at https://www.pnas.org/lookup/suppl/doi:10.1073/pnas.2016037118/-/DCSupplemental.

Published January 18, 2021.

(DSC), small-angle neutron scattering (SANS), and Laurdan fluorescence spectra to extract information on the structure and the thermodynamics. Moreover, we directly visualized the changes on the membranes at the micrometric scale using epifluorescence microscopy.

Results

Our experimental results focus on two main aspects of styrene oligomer–lipid interaction: First, we employed SANS both to confirm the presence of the oligomers within the lipid membrane and to obtain information about the changes on the bilayer structure they induce. Subsequently, we focused on changes in the thermodynamics properties and phase behavior of the membrane caused by inclusion of these short styrene chains.

Fluid and Gel Phases of 1,2-Dipalmitoyl-*sn*-Glycero-3-Phosphocholine Lipid Membranes Can Host a High Amount of Styrene Oligomers. For SANS, we utilized liposomes formed either of 1,2-dipalmitoyl-*sn*-glycero-3-phosphocholine (DPPC) in D_2O as a solvent, to maximize scattering contrast, or d_{62}-DPPC (DPPC lipids with all of the hydrogen molecules in the carbon chains replaced by deuterium) vesicles in a H_2O/D_2O mixture to mask the signal from the lipids and maximize polymer signal. In both lipidic compositions we compared changes between lipid-only liposomes and liposomes formed with 30% mol of styrene oligomers, and scattering curves were acquired at both 20 °C and 50 °C to investigate the differences between gel and fluid phase. Herein we report a brief description of the results; a more comprehensive analysis of the SANS data can be found in *SI Appendix*. Fig. 1 shows the scattering curves of DPPC:SO 70:30 and d_{62}-DPPC:SO 70:30 with their respective model fitting. In the case of DPPC:SO (Fig. 1 *A* and *B*), we observe a good agreement between our data and a bilayer model, particularly for scattering curves at 50 °C (Fig. 1*B*). Contrarywise, for DPPC:SO at 25 °C the fitting strongly deviates from the scattering curve in the intermediate region, indicating a membrane structural change occurring in the gel phase due to the presence of SO. A similar feature has been reported before by Pencer et al. (19) for membranes displaying liquid domain coexistence, and they suggested that changes in the scattering curve in that region might be linked to membrane lateral segregation and heterogeneities in scattering length density. The fitting deviates in the intermediate q region. The good values of model fitting for the DPPC:SO system suggest that upon incorporation of oligomers we still maintain a liposomal suspension with no additional structures, such as aggregates or micelles. This result was also confirmed via dynamic light scattering (DLS), where we observe one single peak in the size distribution of the liposomes (*SI Appendix*, Fig. S6). Scattering curves for d_{62}-DPPC vesicles further confirm the presence of styrene oligomers within the membrane. Fig. 1 *C* and *D* shows the data obtained when the lipid signal is masked. The clear increase in scattering intensity in systems containing SO compared to d_{62}-DPPC-only vesicles (Fig. 1 *C* and *D*, *Insets*) is due to the presence of oligomers in the membrane.

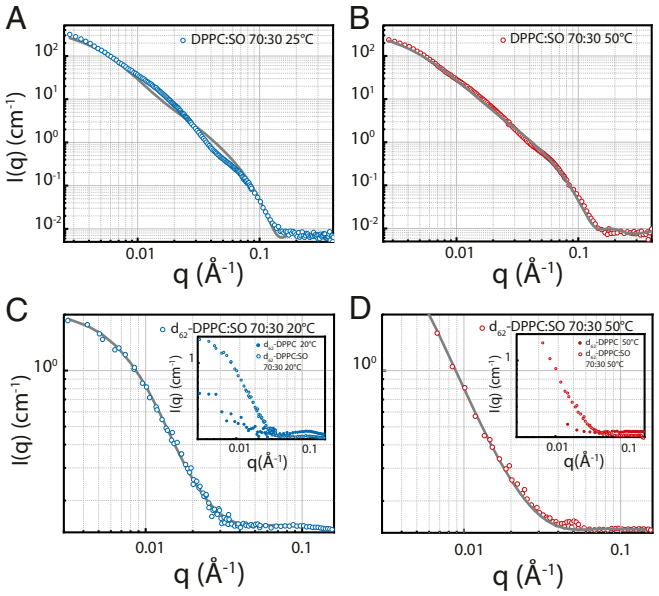

Fig. 1. SANS scattering curves for 50-nm LUVs and relative fittings. (*A*) Fitting with a bilayer model of DPPC:SO scattering curves at 25 °C. (*B*) Fitting with a bilayer model of DPPC:SO scattering curves at 50 °C. (*C*) Fitting of SANS scattering curves for d_{62}-DPPC:SO 70:30 at 20 °C. *Inset* shows comparison of scattering signal between d_{62}-DPPC and d_{62}-DPPC:SO liposomes at 20 °C. (*D*) Comparison of d_{62}-DPPC and d_{62}-DPPC:SO liposomes at 50 °C. *Inset* shows comparison of scattering signal between d_{62}-DPPC and d_{62}-DPPC:SO liposomes at 50 °C. All plots are represented as experimental data (circles) and relative fitting (gray line). Both fittings for *C* and *D* were performed using the Sasfit implemented thin disk model. The signal arising from the pure lipid samples displays very low intensity due to the matching of scattering density between solvent and lipids. In the case of 20 °C, the signal appears slightly more intense due to changes in the scattering length density of lipids.

Phase Changes of the Lipid Bilayer Result in Styrene Oligomer Reorganization. To better understand the oligomer distribution within the lipid bilayer in both the gel (S_o) and fluid (L_α) phases, we extrapolated the structural data for the bilayer under lipid-masking conditions in the presence of styrene oligomers. Fitting of the experimental curves was performed using a disk model, motivated by previous analyses of phase separation in model membranes using SANS, where domains were fitted using a similar form factor (20), and obtained good agreement with the data (Fig. 1 *C* and *D*). We observe that in the gel phase polystyrene appears to aggregate with an average diameter of 349 ± 0.3 Å, smaller than the liposome size, and with a thickness of 38.3 ± 0.1 Å, comparable to the hydrophobic region of the bilayer. The fitting values are compatible with a heterogenous lateral distribution of the polymer, as was hinted by the strong deviation from a bilayer scattering in DPPC:SO in D_2O (Fig. 1*A*). Moreover, the resulting thickness is comparable with the values obtained for DPPC using a model-free approach (Kratky–Porod and Modified Kratky–Porod at 25 °C (*SI Appendix*, Figs. S3 and S4). In the case of the polymer distribution in the fluid phase, we argue that the lack of a visible inflection point in the scattering curve for 50 °C reflects a change in lateral distribution of the polymer, which becomes more homogeneously dispersed within the bilayer, and not a real change in diameter of the vesicles. However, since it was not possible to verify the values for the diameter of the disk, we took into consideration only the value for the thickness, which resulted to be 34.0 ± 0.1 Å. This is once again comparable with the bilayer thickness obtained for DPPC:SO liposomes (*SI Appendix*, Table S1), hinting that both in the gel and in the fluid phase the polymer is intercalated in the acyl chains.

Vesicles Containing SO Have Higher Membrane Order. The Laurdan emission spectra for DPPC liposomal suspensions containing increasing molar fractions of SO (*SI Appendix*, Fig. S7), and the calculated corresponding general polarization (GP) values for each temperature probed (Fig. 2*A*), highlight changes in the membrane order upon incorporation of the oligomers. The GP values obtained for pure DPPC liposomes in the gel and the fluid phase are consistent with previously reported GP curves for DPPC (21), with a GP in the gel phase remaining almost constant

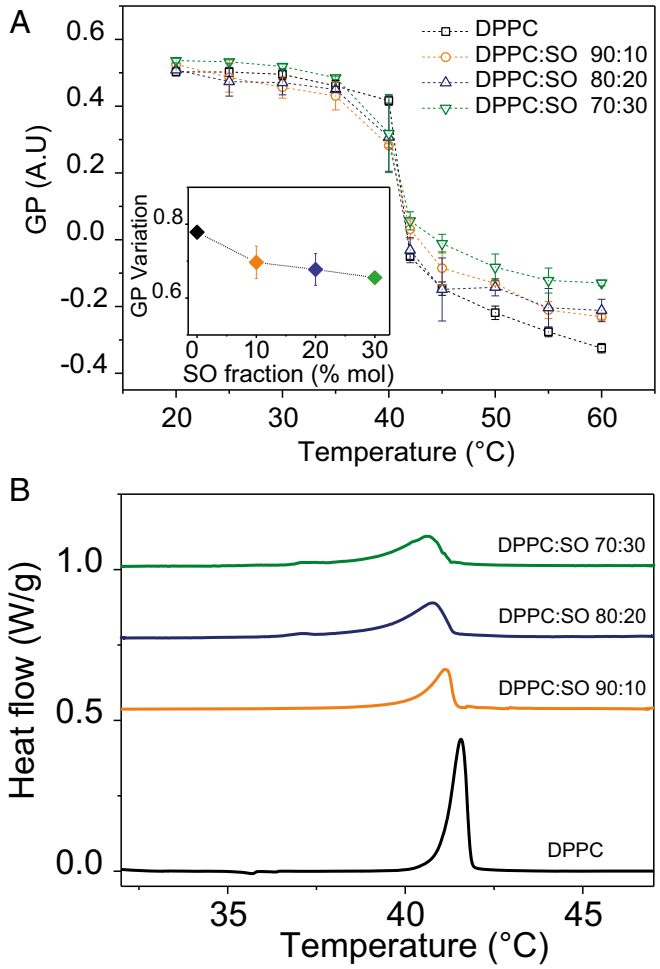

Fig. 2. (*A*) GP curves over temperature for LUVs of DPPC formed in water at 0% (black squares), 10% (orange circles), 20% (blue triangles), and 30% (green inverted triangles) molar fraction of styrene oligomers. *Inset* shows the variation of GP between fluid and gel phase for each SO molar fraction, calculated as ΔGP = GP[50 °C] − GP[20 °C]. Liposomes were extruded to a size of 100 nm. Each data point and error bars represent the average and standard deviation from three (n = 3) separate samples, with four technical repeats each. (*B*) DSC thermographs of DPPC MLVs containing increasing amounts of styrene oligomers. Each curve represents the second thermographic signal from the full run experiment. Thermographs provide a determination of the melting temperature T_m (maximum), enthalpy of melting ΔH (area comprised between the baseline and the peak), and transition width $T_{1/2}$ (half height width).

at 0.50 ± 0.01, and with a sharp decrease after T_m, to a negative value of -0.33 ± 0.01 at 60 °C. Incorporation of the polymer in the membrane does not significantly induce any variation at low temperatures, with a slight increase to 0.54 ± 0.01 for 30% molar fraction of styrene oligomers being observed. In contrast, presence of the polymer strongly shifts the GP to more positive values in the fluid phase, up to -0.13 ± 0.01 for the maximal polymer fraction investigated. We observe a clear dependence of the GP variation on the polymer content (Fig. 2 *A*, *Inset*) that we here argue is due to a uniform distribution of the oligomers within the membrane. The difference in variation of GP, minimal in the gel phase and maximal for the liquid crystalline phase, indicates a different behavior of the polymer between the S_o and L_α. Laurdan spectral properties in different phases of the bilayer have been directly linked to the hydration in the glycerol backbone region of the lipids and to the degree of tail alignment (22). Therefore, the increase in GP suggests a lower number of water molecules in the fluid phase of the bilayer due to the presence of polystyrene, hinting also at a higher packing order of the lipids induced by SO. Such an effect might be indicative of intercalation of styrene oligomers through the lipid chains in the fluid phase. A similar effect was reported for incorporation of hydrophobic monoterpenes, where there was an increase of the order parameter of the acyl chains, particularly the carbon groups closer to the interface (23). In the case of styrene oligomers, the lack of a hydrophilic headgroup prevents the polymer from being exposed to the water–acyl chain interface; however, the observed shift in GP, indicative of a higher order of the chain closer to the headgroup region, suggests that at least a significant portion of the oligomers is not confined in the midplane of the hydrophobic region. This picture is consistent with neutron scattering results reported by Richter et al. (24) in the case of styrene monomers interacting with the 1,2-dimyristoyl-*sn*-glycero-3-phosphocholine vesicle, where the distribution of the monomers was found to be a coexistence of molecules highly segregated in the midplane and molecules aligned with the hydrocarbon tails.

Gel-to-Fluid Transition Is Inhibited by Styrene Oligomers. We employed differential scanning calorimetry to measure the gel-to-fluid transition, specifically changes in the enthalpy and transition temperature which could hint at effects on the membrane induced by styrene oligomers. DSC thermographs (Fig. 2*B*) show for DPPC-only bilayers a sharp transition peak centered at 41.8 ± 0.2 °C, in good agreement with data from the literature (25). With an increasing amount of styrene oligomers incorporated the transition temperature slightly decreases, to a final value of 40.8 ± 0.4 °C for 30% polymer molar fraction. The peak also significantly decreases in intensity and broadens, suggesting a loss in enthalpy and cooperativity. Calculations of ΔH of the transition yield a value of 38.5 ± 0.6 kJ·mol^{-1} for pure DPPC, consistent with previously reported data (25). Incorporation of polymer within the bilayer results in a decrease of enthalpy and cooperativity with increase of the amount of styrene oligomers, as shown in Table 1 and *SI Appendix*, Fig. S8. In particular, we observe a linear decrease of ΔH and increase of $T_{1/2}$ with respect to polymer content, whereas T_m does not vary significantly (*SI Appendix*, Fig. S9). Our results differ significantly from the previously reported trend for dioctadecyldimethylammonium bromide vesicles incorporating 60% molar fraction of styrene monomers, where a strong decrease in transition temperature and only slight variation of enthalpic contribution were observed (17). However, the effects we observe of decrease in T_m and broadening of the transition peak are in agreement with previously reported studies of incorporation of hydrophobic molecules in lipid bilayers (26, 27).

The overall trends of depression of the melting temperature and broadening of the transition are consistent with the effects reported for hydrophobe/lipid bilayer interactions. Wolka et al. (28) and Rolland et al. (26) reported that incorporation of penetration enhancers reduces the transition temperature of DPPC to 40 °C at 10% molar fraction of molecule, as well as causing a significant increase in the width of the transition peak. Similar results have been found for membranes containing flavonoids, with increasing hydrophobicity of the molecule producing a stronger effect (29, 30). Borsacchi et al. (31) also reported similar behavior for incorporation of pheromones in 1,2-dioleoyl-*sn*-glycero-3-phosphocholine (DOPC) bilayers.

Styrene Oligomers Increase Miscibility between S_o and L_α Phases. To better understand the effects induced by the styrene oligomers on the phase behavior of lipid bilayers, we probed changes in the Laurdan spectra in liposomes composed of DOPC and DPPC at different compositions (*SI Appendix*, Fig. S9). Calculation of general polarization yielded GP curves illustrated in

Table 1. Calculated ΔH, T_m, and $T_{1/2}$ for DPPC with increasing molar fractions of styrene oligomers

Styrene oligomers fraction, % mol	ΔH, kJ·mol^{-1}	T_m, °C	$T_{1/2}$, °C
0	38.5 ± 0.7	41.8 ± 0.2	0.27 ± 0.01
10	30.7 ± 3.8	41.5 ± 0.4	0.29 ± 0.01
20	27.9 ± 1.1	41.2 ± 0.3	0.45 ± 0.01
30	25.1 ± 0.9	40.8 ± 0.4	0.66 ± 0.01

Values are presented as average and standard deviation from two (n = 2) separate samples, with six technical repeats each.

Fig. 3. For pure DOPC:DPPC liposomes we observe a broad transition, starting from a value of 0.27 ± 0.01 and 0.45 ± 0.01 at 15 °C to −0.25 ± 0.02 and −0.21 ± 0.01 at 45 °C for DPPC molar fractions of 0.4 and 0.6, respectively. The values at low temperature are much lower than the GP of pure DPPC bilayer (21), indicating a gel/fluid phase coexistence. The miscibility temperature T_m, measured from the intersection of GP curves obtained from excitation wavelengths 350 and 400 nm (*SI Appendix*, Fig. S10), is approximately 28.3 ± 1.5 °C for X_{DPPC} = 0.4 and 34.9 ± 0.9 °C for X_{DPPC} = 0.6, consistent with known values of miscibility for this system (32–36). The values of GP and curve broadness are in agreement with a membrane displaying L_d/S_o coexistence at low temperature and a homogeneous liquid disordered phase above T_m. In the case of systems with the same lipid ratio and additional incorporation of styrene oligomers, we observe significant changes in the Laurdan GP values. For 0.4 DPPC molar fraction the initial value is highly increased to 0.33 ± 0.01 at 15 °C, as well as the value in the liquid crystalline phase which displays higher GP, with a value of 0.22 ± 0.02 at 45 °C. Moreover, the transition temperature decreases to 23.4 ± 0.8 °C and the curve becomes sharper. Increasing the fraction of DPPC in the membrane seems to slightly reduce these effects, as for X_{DPPC} = 0.6 the initial values of GP are comparable, while at 45 °C we observe a slight increase to −0.16 ± 0.02.

We further confirmed the lowering of the liquidus line observed in the GP plots upon addition of 10 mol% SO, by analyzing under epifluorescence microscopy the area coverage of gel phase domains in giant unilamellar vesicles (GUVs) composed of different ratios of DOPC and DPPC. Giant unilamellar vesicles at both DOPC:DPPC compositions display fluid/gel coexistence at room temperature, with characteristic S_o domains of irregular or hexagonal morphology (Fig. 4), consistent with previous reported studies (35). For each vesicle we calculated first the area fraction of S_o domains, f_b, in the pure lipid case, and obtained a total area coverage of 0.17 ± 0.03 and 0.47 ± 0.03 for DPPC molar fraction of 0.4 and 0.6, respectively. It is possible to compare measured values for area coverage with theoretically predicted fractions of gel phase by the lever rule, benefiting from the almost vertical shape of the solidus line in this region of the phase diagram (32). Assuming thus a constant solidus line at 0.95 for the considered DPPC molar fraction interval, our values are consistent with theoretical predictions (Table 2), as well as with previously reported coverage of DPPC gel domains in DOPC membranes (35). Since the S_o fraction in GUVs agrees with DOPC:DPPC phase diagrams, we can now measure the gel phase coverage upon addition of 10 mol% of styrene oligomers, while maintaining the same DOPC:DPPC composition. This overall allows to obtain an experimental phase diagram by combining the values obtained by Laurdan and GUVs. Vesicles incorporating 10% mol SO still exhibit S_o/L_α coexistence, with intact domain morphology (Fig. 4); however, the solid domain fraction, f_b^{SO}, is greatly reduced. Analysis of the domain coverage yielded a fraction

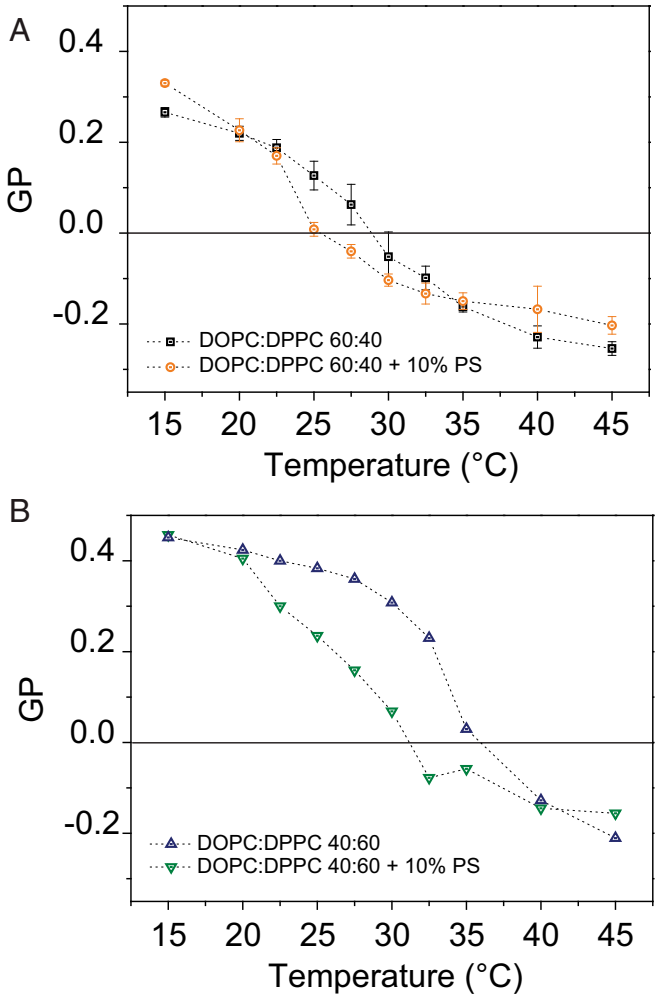

Fig. 3. (*A*) Variation of general polarization over temperature for LUVs of DOPC:DPPC 60:40 (black squares) and DOPC:DPPC 60:40 + 10 mol% SO (orange circles). (*B*) Variation of general polarization over temperature for LUVs of DOPC:DPPC 40:60 (blue triangles) and DOPC:DPPC:SO 40:60 + 10 mol% SO (green inverted triangles). Liposomes were extruded to a size of 100 nm. Each data point and error bars represent the average and standard deviation from two (n = 2) separate samples, with four technical repeats each.

for the solid phase of 0.077 ± 0.021 and 0.28 ± 0.06 for 60:40 and 40:60 mixtures, respectively. The values of solid area fraction obtained with GUVs containing SO allow us to estimate the liquidus line in presence of 10% mol oligomers. For that reason, we have visualized GUVs containing styrene oligomers at two separate temperatures, namely 20 °C and 23 °C. Using a solidus line value for each temperature based on previously reported data by Schmidt et al. (32), and using the lever rule, we obtained values for X_a^{SO} of 0.35 ± 0.05 for 20 °C and 0.38 ± 0.06 for 23 °C. We observe that the miscibility temperatures obtained both from Laurdan spectra and from GUVs confirm the lowering of the liquidus line between S_o-L_α coexistence and pure L_α phase (Fig. 5).

A Theoretical Model Explains the Changes in DOPC:DPPC Miscibility. Furthermore, we compared our experimental results with a thermodynamics model for binary phase diagrams developed by Wolff et al. (36), which considers the gel-to-liquid transition in the framework of a mean-field Ising (two states) model. Simply, for a binary lipid mixture the thermodynamics

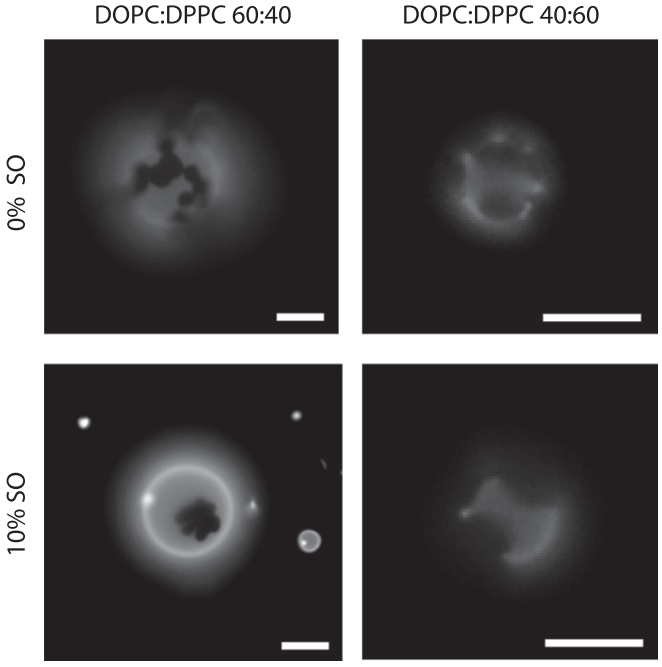

Fig. 4. Representative images of DOPC:DPPC GUVs labeled with 1 mol% DiI, without and with 10 mol% fraction of SO incorporated, visualized using epifluorescence microscopy. The bright area represents presence of fluorophore, which partitions in the L_α phase. Dark spots are S_o domains. The 60:40 vesicles with and without SO were imaged at 20 °C, and 40:60 systems with and without SO were imaged at 23 °C. (Scale bars, 5 μm.)

of the gel-to-liquid transition of a binary mixtures can be written as

$$\begin{aligned}\mathcal{G}^{\mathrm{mix}}(T,\phi_1,\phi_2,m) = &-m[h_1(T)\phi_1 + h_2(T)\phi_2] - 2Jm^2 \\ &+ (\tfrac{1+m}{2})\ln(\tfrac{1+m}{2}) + (\tfrac{1-m}{2})\ln(\tfrac{1-m}{2}) \\ &+ \phi_1\ln(\phi_1) + \phi_2\ln(\phi_2)\end{aligned} \quad [1]$$

with

$$h_1(T) = \frac{\Delta H_1}{2RT_1^2}(T - T_1),\ h_2(T) = \frac{\Delta H_2}{2RT_2^2}(T - T_2), \quad [2]$$

where ϕ_1 and ϕ_2 are the area fractions of the two lipid species, J is the mismatch energy associated with the interaction between two neighboring lipids, m is a nonconserved scalar order parameter restricted to the interval $[-1, 1]$, R is the gas constant, ΔH_1 and ΔH_2 are the respective gel-to-liquid enthalpies of melting, and T_1 and T_2 are the respective transition temperatures. Changes in area per lipid at the transition are not taken into account. The thermodynamic potential $\mathcal{G}^{\mathrm{mix}}$ represents the ratio $G/\mathcal{A}_l RT$ of the Gibbs free energy of mixing of the hydrated lipid bilayer divided by the total area of lipids $\mathcal{A}_l$ and temperature T, while m interpolates continuously between negative (gel state) and positive (fluid state) values. Phase coexistence results from minimization of $\mathcal{G}^{\mathrm{mix}}$ with respect to m followed by convex minimization with respect to ϕ_1 and ϕ_2.

For DOPC:DPPC bilayers we calculated the phase diagram using values of $\Delta H^{\mathrm{DPPC}} = 38.5\ \mathrm{kJ{\cdot}mol^{-1}}$ and $T_m^{\mathrm{DPPC}} = 41.8\,^\circ\mathrm{C}$ for DPPC, obtained from our DSC experiments, and $\Delta H^{\mathrm{DOPC}} = 7.7\ \mathrm{kJ{\cdot}mol^{-1}}$ and $T_m^{\mathrm{DOPC}} = -21.3\,^\circ\mathrm{C}$ obtained from the literature. The mismatch energy of the interaction between neighboring lipids was set at $J = 0.31$. The theoretical model is in good agreement with our experimental data from Laurdan emission spectra and with the DOPC:DPPC phase diagram reported by Chen and Santore (35) (Fig. 5).

For systems containing styrene oligomers, we kept all model parameters constant, except for the different enthalpy and transition temperature obtained from calorimetry experiments, namely $\Delta H^{\mathrm{DPPC:SO}} = 30.7\ \mathrm{kJ{\cdot}mol^{-1}}$ and $T_m^{\mathrm{DPPC:SO}} = 41.5\,^\circ\mathrm{C}$, to calculate the new boundary line. The boundary line in presence of styrene oligomers indeed shows good agreement with our experimental observation (Fig. 5). This suggests that the thermodynamic changes induced by SO in DPPC bilayers are the main driving force behind depression of the liquidus line toward lower temperature.

Conclusions

Our results show that the incorporation of styrene oligomers in lipid bilayers is strongly coupled to membrane phase behavior. In the low temperature gel phase, styrene short chains are laterally segregated in the membrane, as shown by SANS experiments. This segregation is due to the poor solubility of the oligomers in the tightly packed acyl chain region. Neutron scattering experiments also show that, as the bilayer melts from the gel to the L_α phase upon an increase of temperature, the oligomers become more uniformly distributed and intercalate between the acyl chains toward the water interface. This scenario is also supported by the strong variation of GP in the fluid phase, as well as by the close to linear dependence with polymer content of the Laurdan emission and of the transition enthalpy. Incorporation of the oligomers was also found to alter the gel-to-liquid main transition and the lipid packing of the membrane in the fluid phase, as shown by the Laurdan emission spectra. These changes can be ascribed to a preferential partition of the styrene chains into the fluid phase, thus depressing the gel-to-fluid transition temperature of the membrane. The evolution of the thermodynamic coexistence lines between pure bilayers and bilayers containing the short styrene chains is correlated with the change in enthalpy at the gel–fluid transition. In the case of the binary lipid system DOPC:DPPC the presence of the styrene oligomers shifts the S_o and L_α miscibility line toward lower temperatures: Incorporated styrene oligomers have thus the potential to preclude domain formation. Our findings demonstrate that the presence of styrene chains in lipid bilayers affects the membranes' phase behavior and point to a likely disruption of biomembranes' functionality by polymeric nanopollutants.

Materials and Methods

Materials. Chloroform solutions of DOPC (1,2-dioleoyl-*sn*-glycero-3-phosphocholine, $C_{44}H_{84}NO_8P$, M_w 786.11) and DPPC (1,2-dipalmitoyl-*sn*-glycero-3-phosphocholine, $C_{40}H_{80}NO_8P$, M_w = 734.039) were purchased from Avanti Polar Lipids. DiI stain (1,1′-dioctadecyl-3,3,3′,3′-tetramethylindocarbocyanine perchlorate $C_{59}H_{97}ClN_2O_4$, M_w = 933.8793) was provided by ThermoFisher Scientific. Sucrose ($C_{12}H_{22}O_{11}$, M_w = 342.3) and Laurdan (6-dodecanoyl-*N*,*N*-dimethyl-2-naphthylamine) were purchased from Sigma-Aldrich. Atactic styrene oligomers ($(C_8H_8)_n$) M_n = 500 Da) were purchased from Polymer Source Inc. All chemicals had

Table 2. Summary of S_o area coverage for DOPC:DPPC GUVs at different composition

DPPC molar fraction	Experimental S_o fraction (f_b)	Theoretical fraction pure DPPC	Theoretical fraction 0.95 DPPC	S_o fraction with 10% SO (f_b^{SO})
0.4	0.17 ± 0.03	0.18 ± 0.01	0.20 ± 0.01	0.08 ± 0.02
0.6	0.47 ± 0.03	0.42 ± 0.01	0.47 ± 0.01	0.28 ± 0.06

Each value represents average and standard deviation of two separate samples of 40 vesicles each. Vesicles with 0.4 DPPC molar fraction with and without SO were imaged at 20 °C, and systems with 0.6 DPPC molar fraction with and without SO were imaged at 23 °C.

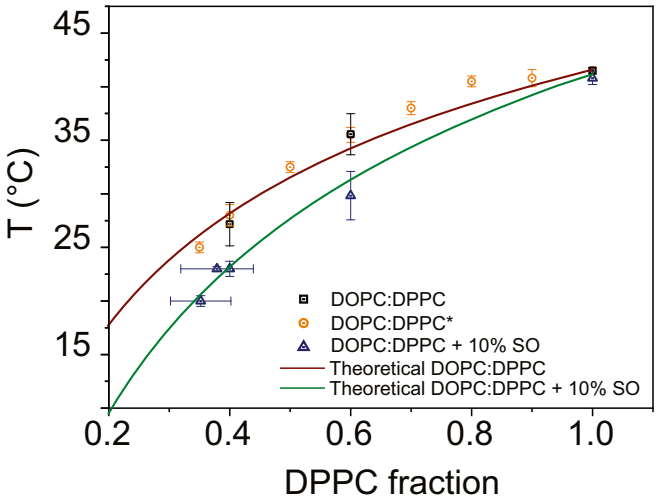

Fig. 5. Comparison between experimental data points for the liquidus line estimated by results from Chen and Santore (35) (orange), experimental data points for DOPC:DPPC (black squares) and DOPC:DPPC:SO (blue triangles) obtained from Laurdan emission spectra, and theoretical predictions of liquidus lines for DOPC:DPPC (red) and DOPC:DPPC + 10% SO (green).

high purity and were used without further purification. The osmolarities of the sucrose solutions were measured with a cryoscopy osmometer (Osmomat 030; Gonotec).

Multilamellar Vesicles and Large Unilamellar Vesicles (LUVs) Preparation. For DSC experiments, multilamellar vesicles (MLVs) were prepared by placing 1.5 mg of the desired lipid (with and without styrene oligomers) composition in chloroform in a glass vial, and organic solvent was evaporated using first an argon stream for 20 min, followed by 8 h of vacuum pumping. The lipid film was then hydrated with MilliQ distilled water (18.2 MΩ) at 70 °C to reach the desired concentration and gently vortexed. The resulting MLV suspensions were sonicated for 15 min to disperse larger aggregates. In the case of Laurdan measurements, large unilamellar vesicles (LUVs) were prepared similarly to the MLV protocol with the following modifications. The lipid solution in chloroform was mixed with 1 mol% Laurdan in chloroform prior to evaporation. Upon swelling with MilliQ water and sonication, the MLV solution was extruded using an Avanti Mini-Extruder 21 times through a 100-nm diameter pore polycarbonate filter.

Small Unilamellar Vesicles Preparation. Liposomes of the desired lipid composition were formed using MilliQ distilled water (18.2 MΩ), H_2O/D_2O 92:8, or D_2O. For fluorescence measurements, the lipids were stained with 1 mol% Laurdan in chloroform prior to evaporation. Liposomal solutions remained stable over a period of days. In the case of liposomal suspension used in SANS experiments liposomes were then extruded using an Avanti Mini-Extruder. The sample was first extruded 21 times through 200-nm diameter, subsequently 21 times through 100-nm diameter, and finally 21 times through 50-nm diameter pore polycarbonate filters.

SANS. The neutron wavelength resolution was $2 \cdot \Delta\lambda/\lambda = 0.1$. All scattering data were corrected for background, and incoherent scatterings from 1-mm-thick D_2O or H_2O solutions were used to correct for the deviation in uniformity of the detector response. The final data were converted to absolute scale. All experiments were first performed at low temperature (25 °C) and then at 50 °C. SANS measurements for 100% D_2O contrast were performed at 24.0-, 8.0-, and 1.5-m detector distances at the D11 small-angle instrument at Institut Laue-Langevin, Grenoble, France. The wavelength of neutrons was set to 6 Å. The instrument was configured to provide an effective q range of ∼0.01 to 0.4 $Å^{-1}$. All SANS measurements were performed at 20 °C and 50 °C, well above the phase transition temperature of DPPC (∼42 °C). The SANS data from the position-sensitive two-dimensional detector were reduced to one-dimensional profiles I(q) vs. q, by using a facility-supplied data reduction software lamp. Preliminary scattering data and measurements to determine the contrast matching conditions were obtained on the PACE spectrometer at the Laboratory Leon Brillouin (LLB) in Saclay, France.

Steady-State Fluorescence. A total of 3 mL of liposomal suspension stained with Laurdan of total concentration 3 mg/mL was placed in a quartz silica cuvette with 1-mm path length. Acquisition of Laurdan emission spectra was performed with a Jobin Horiba FluoroMax equipped with a Peltier unit to control temperature. Excitation wavelength was set at 350 nm with a bandpass of 1 nm and emission was also recorded with slit of 1 nm. The solution was equilibrated at a given temperature for 10 min before each acquisition. For DPPC:SO Laurdan experiments, each sample (n = 3) was probed for two cycles of heating and cooling. For DOPC:DPPC:SO LUVs experiments, we performed two cycles of heating and cooling at excitation 350 nm and one cycle of heating and cooling at excitation 400 nm on two (n = 2) separate samples. GP was calculated using the standard expression provided by Parasassi et al. (37). To quantify the miscibility temperature for each sample, we compared the GP plot from excitations 350 and 400 nm and extrapolated the temperature range at which the two curves intersect. A full description of quantification is provided in *SI Appendix*.

Giant Unilamellar Vesicles Preparation. GUVs composed of DOPC:DPPC, both in absence and presence of styrene oligomers, were prepared by electroformation following the protocol introduced by Angelova and Dimitrov (38). Simply, 5 μL of 2 mg/mL solution of DOPC:DPPC or DOPC:DPPC:SO at the desired molar ratio, stained with 1% mol of DiI, in chloroform was spread on each cathode of a custom-made electroformation stage. The stage was kept under vacuum for at least 1 h to ensure complete evaporation of solvent and subsequently the lipid film was hydrated using sucrose solution (100 mosm/kg) at 55 °C. We applied a sinusoidal electric field of 1-V peak–peak intensity at 10 kHz for 1 h while keeping the sample heated above the transition temperature. The resulting GUV suspension was kept at 20 °C in a water bath to ensure complete stabilization of the sample. Vesicles were used on the same day of preparation.

Optical Microscopy and S_o Phase-Domain Quantification. Imaging of GUVs labeled with 1 mol% DiI was performed using a Nikon Eclipse TE2000-E microscope equipped with a Diagnostic Instruments NDIAG1800 camera and a Nikon 60× water immersion, NA 1.2 objective. Observation was performed in the epifluorescence mode with a Hg lamp, with 100 W (Intensilight; Nikon) as excitation source and adapted filtering TE/TRITC Ex 543/22 nm, DM 562 nm, and Em 593/40 nm. GUV samples were initially swelled by diluting the external medium with ∼5 vol% of pure water. Prior to experimental observation, GUVs were kept at the desired temperature for at least 1 h to stabilize. A total of 100 μL of a GUV solution was placed in a chamber. Quantification of S_o phase domains in vesicles was performed by measuring the radius of the domains, which was then corrected for by taking into account the spherical nature of the GUVs. A more detailed description of the quantification approach can be found in *SI Appendix*. For each lipid composition we quantified the domain area coverage from two separate samples, with 40 vesicles from each replicate.

Differential Scanning Calorimetry. The calorimetry measurements were performed with a high-sensitivity differential scanning calorimeter (μDSC; Setaram). The measuring cell was filled with the sonicated sample, while the reference cell was filled with MilliQ water. The temperature of the cells was changed with a constant rate (heating rate, 0.5 $K \cdot min^{-1}$; cooling rate, 0.3 $K \cdot min^{-1}$). The system was equilibrated ∼20 min before each heating or cooling ramp. The analysis of DSC data was performed using OriginPro 9.0. For each sample (n = 2) we performed three cycles of heating and cooling.

DLS. Liposomal suspensions of lipid and lipid:SO vesicles were characterized by dynamic light scattering using a Malvern Zetasizer Nano ZS. Simply, 1 mL of liposomal suspsension at 1 mg/mL was placed in a disposable plastic cuvette and light scattering was recorded. Measurements were repeated at least three times for statistics.

Data Availability. SANS, Laurdan, and DSC are ASCII data files arranged as tables. GUV images are provided as TIFF files. Data have been deposited in Zenodo (DOI: 10.5281/zenodo.4118224).

ACKNOWLEDGMENTS. We thank Prof. Jian Liu (University of Manchester) and Prof. Olivier Sandre (University of Bordeaux) for providing expertise in discussing the neutron scattering results. We also thank Annie Brûlet who provided expertise and assisted in the acquisition of the neutron scattering data at the Leon Brillouin Laboratory (LLB) and the Institute Laüe-Langevin in Grenoble and the LLB in Saclay for providing the facilities needed to conduct the neutron scattering experiment. The ISO9001 Characterization Platform of the Institut Charles Sadron is gratefully acknowledged for

access to the μDSC and fluorometer. M.I.M., M.K., F.T., A.S., and C.M.M. acknowledge funding from the European Marie Skłodowska-Curie Actions of the 7th Framework Program (FP7-MSCA) International Training Network (ITN) 608184 Smart Nano-Objects for Alteration of Lipid Bilayers (SNAL) for support for this work. Portions of this paper were developed from M.I.M.'s PhD manuscript.

1. M. Haward, Plastic pollution of the world's seas and oceans as a contemporary challenge in ocean governance. *Nat. Commun.* **9**, 667 (2018).
2. S. B. Borrelle *et al.*, Opinion: Why we need an international agreement on marine plastic pollution. *Proc. Natl. Acad. Sci. U.S.A.* **114**, 9994–9997 (2017).
3. J. R. Jambeck *et al.*, Plastic waste inputs from land into the ocean. *Science* **347**, 768–771 (2015).
4. M. Piccardo, M. Renzi, A. Terlizzi, Nanoplastics in the oceans: Theory, experimental evidence and real world. *Mar. Pollut. Bull.* **157**, 111317 (2020).
5. B. Gewert, M. M. Plassmann, M. MacLeod, Pathways for degradation of plastic polymers floating in the marine environment. *Environ. Sci. Processes Impacts* **17**, 1513–1521 (2015).
6. M. Cole, P. Lindeque, C. Halsband, T. S. Galloway, Microplastics as contaminants in the marine environment: A review. *Mar. Pollut. Bull.* **62**, 2588–2597 (2011).
7. M. C. Fossi *et al.*, Are baleen whales exposed to the threat of microplastics? A case study of the Mediterranean fin whale (Balaenoptera physalus). *Mar. Pollut. Bull.* **64**, 2374–2379 (2012).
8. A. Collignon *et al.*, Neustonic microplastic and zooplankton in the north western Mediterranean Sea. *Mar. Pollut. Bull.* **64**, 861–864 (2012).
9. K. Mattsson, L. A. Hansson, T. Cedervall, Nano-plastics in the aquatic environment. *Environ. Sci. Processes Impacts* **17**, 1712–1721 (2015).
10. Y. Lu, Y. Mei, R. Walker, M. Ballauff, M. Drechsler, 'Nano-tree'-type spherical polymer brush particles as templates for metallic nanoparticles. *Polymer* **47**, 4985–4995 (2006).
11. E. Bergami *et al.*, Nano-sized polystyrene affects feeding, behavior and physiology of brine shrimp Artemia franciscana larvae. *Ecotoxicol. Environ. Saf.* **123**, 18–25 (2016).
12. M. A. Browne, A. Dissanayake, T. S. Galloway, D. M. Lowe, R. C. Thompson, Ingested microscopic plastic translocates to the circulatory system of the mussel, Mytilus edulis (L). *Environ. Sci. Tech.* **42**, 5026–5031 (2008).
13. M. Al-Sid-Cheikh *et al.*, Uptake, whole-body distribution, and depuration of nanoplastics by the scallop pecten maximus at environmentally realistic concentrations. *Environ. Sci. Tech.* **52**, 14480–14486 (2018).
14. K. Saido *et al.*, New analytical method for the determination of styrene oligomers formed from polystyrene decomposition and its application at the coastlines of the north-west Pacific Ocean. *Sci. Total Environ.* **473–474**, 490–495 (2014).
15. G. Rossi, J. Barnoud, L. Monticelli, Polystyrene nanoparticles perturb lipid membranes. *J. Phys. Chem. Lett.* **5**, 241–246 (2014).
16. D. Bochicchio, E. Panizon, L. Monticelli, G. Rossi, Interaction of hydrophobic polymers with model lipid bilayers. *Sci. Rep.* **7**, 6357 (2017).
17. M. Jung *et al.*, Interaction of styrene with dodab bilayer vesicles. Influence on vesicle morphology and bilayer properties. *Langmuir* **16**, 968–979 (2000).
18. E. Z. Radlinska *et al.*, Polymer confinement in surfactant bilayers of a lyotropic lamellar phase. *Phys. Rev. Lett.* **74**, 4237–4240 (1995).
19. J. Pencer *et al.*, Detection of submicron-sized raft-like domains in membranes by small-angle neutron scattering. *Euro. Phys. J. E* **18**, 447–458 (2005).
20. T. P. T. Dao *et al.*, Phase separation and nanodomain formation in hybrid polymer/lipid vesicles. *ACS Macro Lett.* **4**, 182–186 (2015).
21. L. A. Bagatolli, B. Maggio, F. Aguilar, C. P. Sotomayor, G. D. Fidelio, Laurdan properties in glycosphingolipid-phospholipid mixtures: A comparative fluorescence and calorimetric study. *Biochim. Biophys. Acta Biomembr.* **1325**, 80–90 (1997).
22. S. S. W. Leung, J. Brewer, L. A. Bagatolli, J. L. Thewalt, Measuring molecular order for lipid membrane phase studies: Linear relationship between Laurdan generalized polarization and deuterium NMR order parameter. *Biochim. Biophys. Acta Biomembr.* **1861**, 183053 (2019).
23. Q. D. Pham, D. Topgaard, E. Sparr, Cyclic and linear monoterpenes in phospholipid membranes: Phase behavior, bilayer structure, and molecular dynamics. *Langmuir* **31**, 11067–11077 (2015).
24. A. G. Richter *et al.*, Scattering studies of hydrophobic monomers in liposomal bilayers: An expanding shell model of monomer distribution. *Langmuir* **27**, 3792–3797 (2011).
25. D. Marsh, *Handbook of Lipid Bilayers* (CRC Press, ed. 2, 2013).
26. A. Rolland, A. Brzokewicz, B. Shroot, J. C. Jamoulle, Effect of penetration enhancers on the phase transition of multilamellar liposomes of dipalmitoylphosphatidylcholine. A study by differential scanning calorimetry. *Int. J. Pharm.* **76**, 217–224 (1991).
27. G. Albertini, C. Donati, R. Phadke, M. Ponzi Bossi, F. Rustichelli, Thermodynamic and structural effects of propranolol on DPPC liposomes. *Chem. Phys. Lipids* **55**, 331–337 (1990).
28. A. M. Wolka, J. H. Rytting, B. L. Reed, B. C. Finnin, The interaction of the penetration enhancer DDAIP with a phospholipid model membrane. *Int. J. Pharm.* **271**, 5–10 (2004).
29. F. Ollila, K. Halling, P. Vuorela, H. Vuorela, J. Slotte, Characterization of flavonoid–biomembrane interactions. *Arch. Biochem. Biophys.* **399**, 103–108 (2002).
30. C. Valenta, A. Steininger, B. G. Auner, Phloretin and 6-ketocholestanol: Membrane interactions studied by a phospholipid/polydiacetylene colorimetric assay and differential scanning calorimetry. *Eur. J. Pharm. Biopharm.* **57**, 329–336 (2004).
31. S. Borsacchi *et al.*, Phase transitions in hydrophobe/phospholipid mixtures: Hints at connections between pheromones and anaesthetic activity. *Phys. Chem. Chem. Phys.* **18**, 15375–15383 (2016).
32. M. L. Schmidt, L. Ziani, M. Boudreau, J. H. Davis, Phase equilibria in DOPC/DPPC: Conversion from gel to subgel in two component mixtures. *J. Chem. Phys.* **131**, 175103 (2009).
33. B. R. Lentz, Y. Barenholz, T. E. Thompson, Fluorescence depolarization studies of phase transitions and fluidity in phospholipid bilayers. 2. Two-component phosphatidylcholine liposomes. *Biochemistry* **15**, 4529–4537 (1976).
34. K. Furuya, T. Mitsui, Phase transitions in bilayer membranes of dioleoylphosphatidylcholine/dipalmitoyl-phosphatidylcholine. *J. Phys. Soc. Jpn.* **46**, 611–616 (1979).
35. D. Chen, M. M. Santore, 1,2-dipalmitoyl-sn-glycero-3-phosphocholine (DPPC)-rich domain formation in binary phospholipid vesicle membranes: Two-dimensional nucleation and growth. *Langmuir* **30**, 9484–9493 (2014).
36. J. Wolff, C. M. Marques, F. Thalmann, Thermodynamic approach to phase coexistence in ternary phospholipid-cholesterol mixtures. *Phys. Rev. Lett.* **106**, 128104 (2011).
37. T. Parasassi, E. K. Krasnowska, L. Bagatolli, E. Gratton, Laurdan and Prodan as polarity-sensitive fluorescent membrane probes. *J. Fluoresc.* **8**, 365–373 (1998).
38. M. I. Angelova, D. S. Dimitrov, Liposome electroformation. *Faraday Discuss. Chem. Soc.* **81**, 303–311 (1986).

PNAS
www.pnas.org

Supplementary Information for

Accumulation of styrene oligomers alters lipid membrane phase order and miscibility

Mattia I. Morandi, Monika Kluzek, Jean Wolff, André Schroder, Fabrice Thalmann and Carlos M. Marques

Carlos M. Marques, E-mail: marques@unistra.fr;
Mattia Morandi, E-mail: mattia.morandi@weizmann.ac.il

This PDF file includes:

Supporting Information Text

Neutron scattering intensity curves of pure DPPC and styrene oligomers loaded DPPC:SO liposome systems

SANS experiments were performed on vesicle suspensions of pure lipid and lipid containing short styrene chains. For each sample, we acquired scattering curves at two different temperatures, 25°C and 50°C, to obtain structural information on the gel and fluid phase of the bilayer, respectively. The SANS scattering curves for DPPC and DPPC:SO for both measured temperatures are shown in Fig. S1. To maximize the contrast with the hydrocarbon region and minimize incoherent scattering, we used pure (100%) D_2O as a solvent.

At 25°C in the gel phase (Fig. S1 C), the DPPC curve displays an inflection point at 0.01 $Å^{-1}$, followed by a power-law decrease of scattering intensity in the intermediate region (0.01 $Å^{-1}$-0.07 $Å^{-1}$), with q^{-2} dependence. The kink observed at 0.01 $Å^{-1}$ is consistent with a rather monodisperse liposome dispersion with a typical radius of 50 nm (see Guinier plot below), consistent with the 50 nm pore size used in the extrusion preparation method. Pure DPPC curves at 50°C (Fig. S1 A) display the same kink at 0.01 $Å^{-1}$, showing that crossing the transition between gel and fluid phase does not significantly alter the size distribution of the liposomes.

Incorporation of styrene oligomers results in a suppression of the inflection point (0.01 $Å^{-1}$ at both temperatures, Fig S1 B, and D) suggesting higher liposome size polydispersity in the sample when styrene oligomers are present, irrespective of temperature. Interestingly, incorporation of styrene oligomers in the membrane results in a small inflection located at around 0.04 $Å^{-1}$ in case of polymer-loaded vesicles at 25°C (Fig S1 E), pointing to some modification of the bilayer structure. However, this feature disappears once the temperature is raised above the lipid melting transition, consistent with a more homogeneous distribution of the polymer throughout the bilayer in the fluid phase.

The scattering curves demonstrate that liposome formation upon extrusion is also observed when short styrene oligomers are added to the lipid solution, and the liposome sizes are preserved. However, clear changes in the intermediate scattering regime makes it possible to distinguish among SO free and SO loaded sample.

Guinier regime. We estimated the characteristic radius of gyration (R_g) for each sample using the Guinier approximation. In case of unilamellar vesicles, with only solvent molecules in the interior, the radius of gyration is expected to match the average liposome radius. The radii were determined from the slope of $\ln(I(q))$vs q^2 plot, which were fitted to a linear model in the range $8 \cdot 10^{-3}$ - $1.5 \cdot 10^{-2} Å^{-2}$, as shown in Fig. S2.

$$\ln(I(q)) = \ln(I_0) - \frac{q^2 R_g^2}{3} \quad [1]$$

Using the 4 smallest q values in the Guinier plot, we found for our four samples gyration radius values R_g ranging between 360 and 410 Å(see Table S1). The corresponding products qR_g lie in the range 1.2-1.6. The R_g sizes are consistent with the hydrodynamic diameters deduced from dynamical light scattering (DLS, Fig S6 and Table S1), and also with the radius used in the shell model for fitting the entire q-range intensity curves. Our SANS data are all consistent with the presence of lipid liposomes with a radius of magnitude 400 Å, and suggest that incorporation of SO do not change drastically the size of the extruded vesicles.

Estimation of bilayer thickness. A spherical shell with uniform scattering length density (SLD) can be approximated at large q by a planar sheet (Kratky-Porod regime) (1). The associated scattering intensity curve behaves as:

$$I(q) \propto \left[\frac{2}{q^2} \sin\left(\frac{qd}{2}\right)\right]^2 \quad [2]$$

It follows that in the intermediate regime $d/R_g < qd < 1$ the product $q^2 I(q)$ can be approximated as:

$$q^2 I(q) \propto \left[\frac{2}{q} \sin\left(\frac{qd}{2}\right)\right]^2 \simeq d^2 \left[1 - \frac{q^2 d^2}{12}\right] \simeq d^2 \exp\left(-\frac{q^2 d^2}{12}\right) \quad [3]$$

with $d^2/12$ the section gyration radius of a slab of thickness d. A first value can be obtained by fitting $\ln(I(q))$ *vs* q^2 to a straight line, which is referred as the Kratky-Porod (KP) thickness d_{KP}. A second value can be extracted, assuming that data follow the behavior (2) at q large enough so that $q^4 I(q)$ reaches a maximum at $q_{\max} = \pi/d_{\mathrm{MKP}}$:

$$q^4 I(q) \propto \sin\left(\frac{qd}{2}\right)^2 \quad [4]$$

The resulting thickness d_{MKP} is referred as the Modified Kratky-Porod (MKP) value. Both d_{MKP} and d_{KP} were estimated and are presented in Table S1. They agree within 10%, the MKP being slightly smaller than the KP values, being of the order of magnitude of 40 Å. KP plots are shown in Fig. S3 and MKP plots in Fig. S4. The range of values qd used in the KP fit lies between 1.6 and 2.4. It can be checked numerically that for this range of qd values, the exponential approximation (3) starts to deviate lightly from the sine expression, which may explain the systematic shift between MKP and KP values, already observed by Sreij et al. (2). The estimate for $q_{\max}$ was obtained by fitting $q^4 I(q)$ to a fourth order polynomial in the interval $q^2 \in [0.05, 0.12]$ $Å^{-2}$, and then determining the position of the maximum of the polynomial curve (with an Origin plug-in).

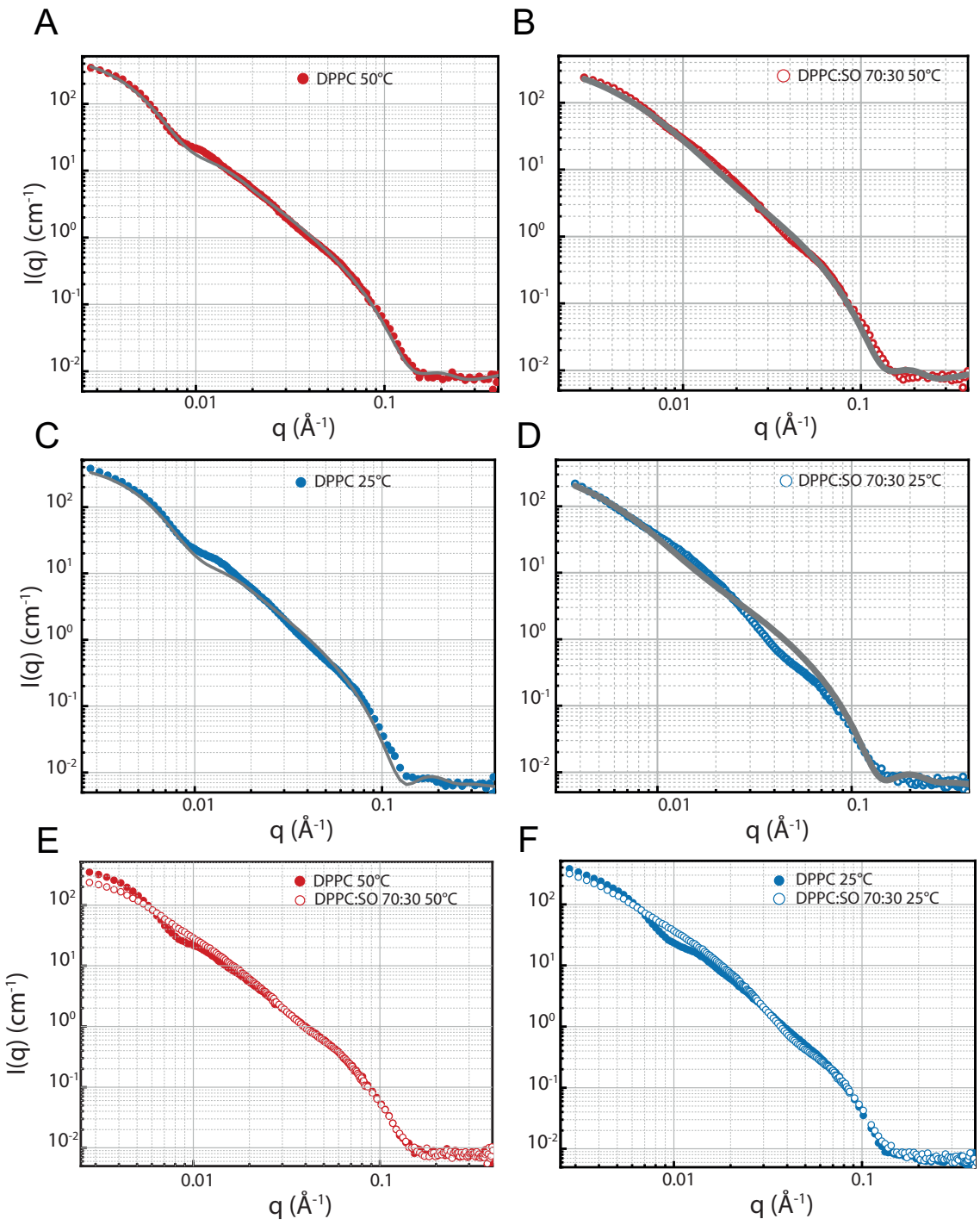

Fig. S1. Small Angle Neutron Scattering (SANS) curves of pure DPPC and DPPC containing 30% styrene oligomers (SO) 50 nm SUVs solution in D_2O, recorded below (25°C) and above (50°C) the melting phase transition of the lipids. (A) SANS intensity curve for pure DPPC liposomes at 50°C (filled red circles) and fit to a spherical shell model (black line, see text for details), (B) SANS intensity for DPPC:SO (70:30) at 50°C (hollow red circles) and fit to a spherical shell model (black line). (C) SANS intensity curve for pure DPPC liposomes at 25°C (filled blue circles) and fit (black line), (D) SANS intensity for DPPC:SO (70:30) at 25°C (hollow blue circles) and fit (grey line). (E) Superimposed DPPC (filled red circles) and DPPC:SO (hollow red circles) intensities at 50°C, (F) superimposed DPPC (filled blue circles) and DPPC:SO (hollow blue circles) intensities at 25°C.

Upon crossing the melting temperature, the KP and MKP bilayer thickness values of pure lipid systems decrease by 10%, as expected from going from a thick gel to a thin fluid lipid phase. Bilayers containing SO seem to behave differently, as their apparent thicknesses hardly change upon crossing the DPPC melting temperature. Addition of 30% SO does not seem to alter the bilayer thickness by a large amount.

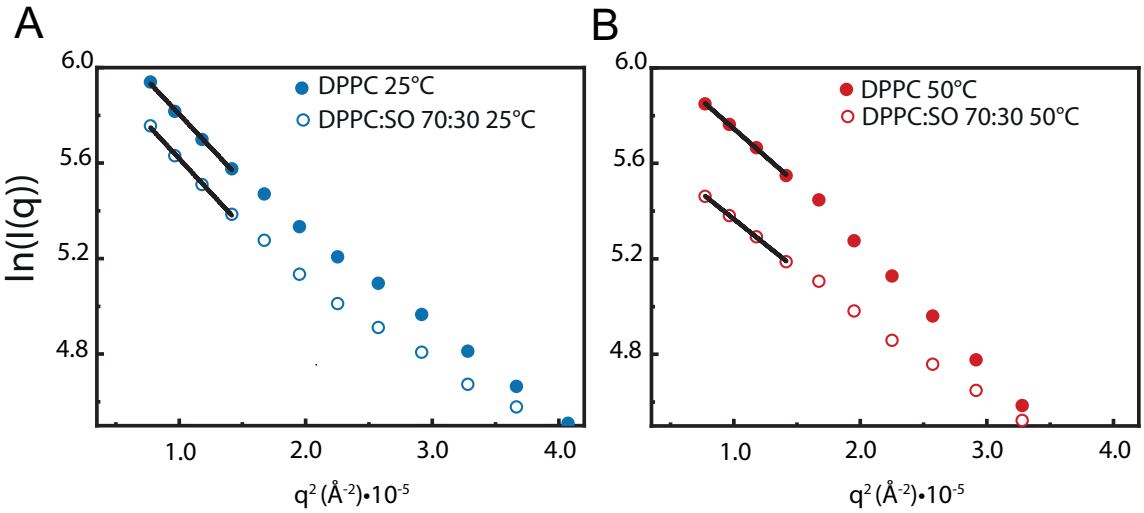

Fig. S2. Guinier plot of DPPC and DPPC:SO 50 nm SUVs at 25°C (A) and 50°C (B). The solid lines represent the best fits to data.

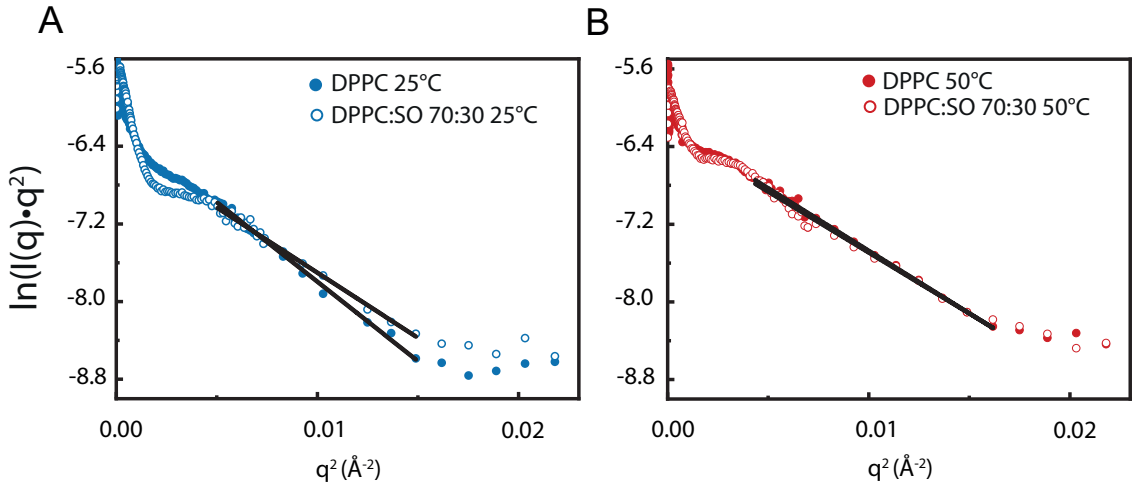

Fig. S3. Kratky–Porod plot of 50 nm SUVs of pure DPPC and 30% SO-DPPC mixtures at 25°C (A) and 50°C (B). The solid lines are linear fittings, according to equation 3.

Table S1. Bilayer thickness calculated by KP and MKP methods, together with radius of gyration obtained via Guinier approximation and diameter obtained from dynamic light scattering (DLS).

SO molar fraction (mol%)	Temperature (°C)	d_{MKP} (Å)	d_{KP} (Å)	R_g (Å)	Average diameter value from DLS (Å)
0	25.	40.4 ± 0.1	44.3 ± 0.7	407 ± 14	818 ± 2
30	25.	36.8 ± 0.1	40.1 ± 1.1	410 ± 14	848 ± 3
0	50.	35.8 ± 0.1	39.3 ± 0.8	375 ± 7	785 ± 2
30	50.	36.7 ± 0.1	39.0 ± 1.0	358 ± 5	773 ± 3

SANS data model fitting

A. . DPPC liposomes in D_2O

We did not expect much mutual vesicle interaction in the range of lipid concentrations used in the experiment, and we therefore neglected the structure factor contribution to the scattering intensity ($S(q) = 1$). A spherical bilayer model was used to model the vesicle form factor $F(q)$. The neutron scattering lengths and molecular volumes of the various components used to calculate the scattering length densities in the model are listed in Table S2.

The SLD of chain regions containing SO was expressed as:

$$\eta_{\mathrm{chain,SO}} = \frac{b_{\mathrm{SO}} \times r_{\mathrm{SO}} + b_{\mathrm{DPPC}} \times r_{\mathrm{DPPC}}}{V_{\mathrm{SO}} \times r_{\mathrm{SO}} + V_{\mathrm{DPPC}} \times r_{\mathrm{DPPC}}} \quad [5]$$

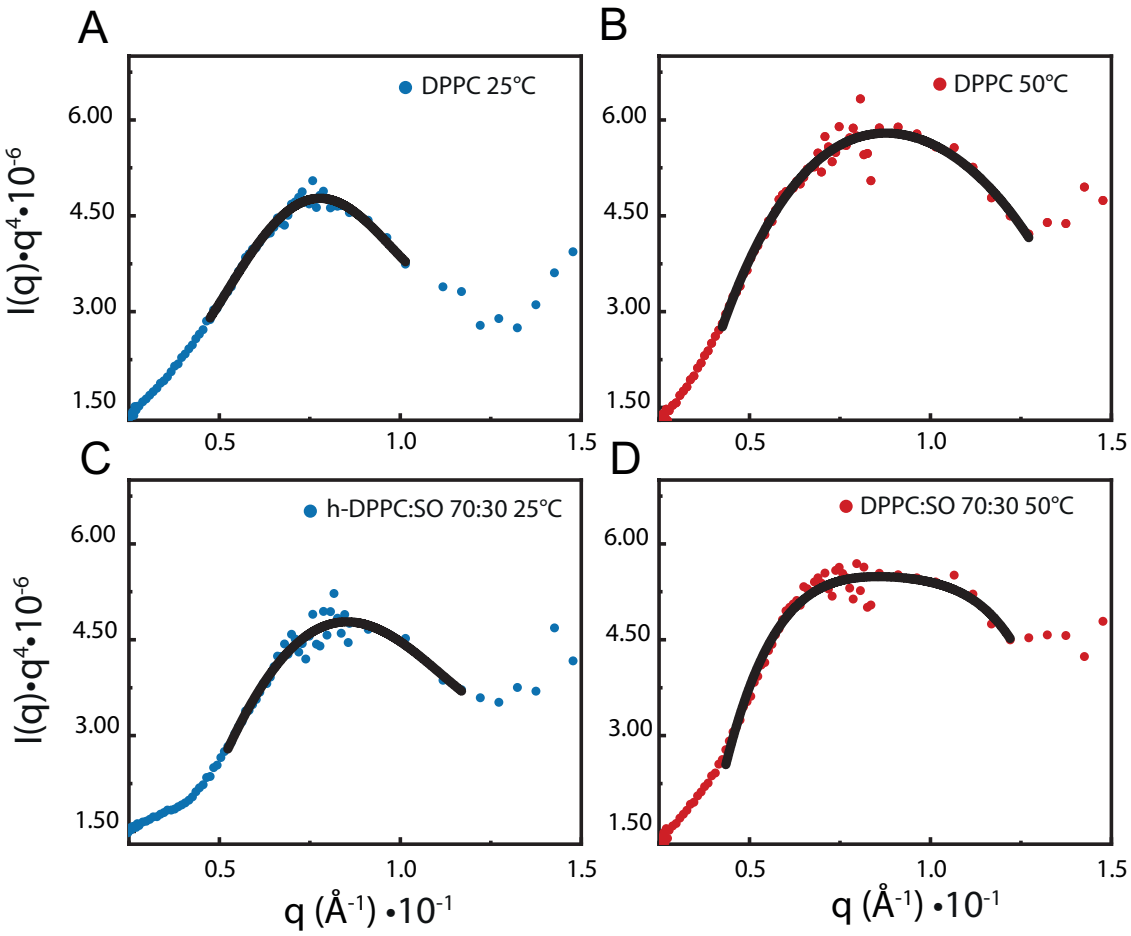

Fig. S4. Modified-Kratky–Porod plot (MKP) of SANS data for 50 nm SUVs of DPPC (A) and DPPC:SO 70:30 (C) at 25°C and DPPC (B) and DPPC:SO 70:30 (D) at 50°C. The solid lines correspond to polynomial fits.

where r_{SO} , r_{DPPC} are the molar fractions of styrene oligomers (SO) and DPPC chains respectively, b_{SO} and b_{DPPC} are the scattering lengths of SO and DPPC chains, V_{SO} and V_{DPPC} the molecular volumes of SO and DPPC chains (derived from the SLD $\eta_{\mathrm{SO}} = 1.414 \times 10^{-6}$ Å^{-2} of pure amorphous styrene oligomers at 23°C (3)). The average degree of polymerisation of the styrene oligomers was taken equal to $n = 4.8$, corresponding to a molecular weight of 500 g·mol^{-1}. It was assumed that mixing was homogeneous, that the molecular volume of SO does not depend on temperature and that no change in specific volume occurs upon mixing. The resulting SLD for a bilayer incorporating 30% SO in the chain region reads:

$$\eta_{\mathrm{chain,SO}} = 1.23 \cdot 10^{-7} \text{Å}^{-2} \quad [6]$$

We also assumed that the component molecular volumes remained unchanged in both gel and fluid phase, which amounts to stating that SO stays homogeneously spread into the lipid bilayer. The scattering intensity of the bilayer vesicle model was calculated using the bilayered model of the SASfit software. It consists in three spherical shells, respectively associated to the inner and outer headgroup regions with uniform SLD η_h, and to the hydrophobic central tail region with SLD η_t. The outer solvent was taken as pure deuterated water with η_{sol}.

$$\begin{aligned} I_b(q) \sim |K(q, R_c, \eta_{\mathrm{sol}} - \eta_h) + K(q, R_c + t_h, \eta_h - \eta_t) + \\ K(q, R_c + t_t + t_h, \eta_t - \eta_h) + K(q, R_c + t_t + 2t_h, \eta_h - \eta_{\mathrm{sol}})|^2 \end{aligned} \quad [7]$$

$$K(q, R, \Delta\eta) = \frac{4\pi R^3}{3} \Delta\eta \; 3 \; \frac{\sin(qR) - qR\cos(qR)}{(qR)^3} \quad [8]$$

where R_c is the radius of the core, t_h the thickness of the headgroup region, t_t the thickness of the tail region, $K(q, R_c, \Delta\eta)$ the volume and SLD weighted form factor of uniform sphere with radius R_c and scattering length density $\Delta\eta$. The computed intensity I_m was convoluted with the instrument resolution function, and the dispersion of the vesicle sizes was approximated by a log-normal distribution. The fitting parameters were the headgroup thickness t_h, the chain thickness t_t and the headgroup scattering length density SLD_h. All three parameters were constrained by reasonable ranges of SLDs, headgroup and chain

Table S2. Molecular volumes V, neutron coherent scattering lengths b_{coh}, scattering length densities η of DPPC lipid and styrene oligomers (SO), used in the model fit

Chemical formula	Description	V (Å^3)	b_{coh} (10^{-5} Å)	η (10^{-6} Å^{-2})
$C_{40}H_{80}NO_8P$	all (h) 50°C	1232.	27.6	0.224
$C_{40}H_{18}D_{62}NO_8P$	all (d_{62}) 50°C	1242.	673.	5.42
$C_{30}H_{62}$	two tails (h) 50°C	913.	-32.5	-0.356
$C_{30}D_{62}$	two tails (d_{62}) 50°C	923.	613.	6.641
$C_{10}H_{18}NO_8P$	headgroup (h)	319.	60.054	1.883
styrene C_8H_8	monomer 104 Da	164.4	23.248	1.414
styrene oligomers $[C_8H_8]_{4.8}$	oligomer 500 Da	791.	111.8	1.414
heavy water	D_2O	30.0	19.14	6.34
water	H_2O	30.0	-1.68	-0.56

Table S3. styrene oligomers fraction x, Temperature T, headgroup region t_h, chain region t_t, bilayer thickness $t_t + 2t_h$, head group SLD

x(SO)(%)	T (K)	t_h (Å)	t_t (Å)	$d = t_t + 2t_h$ (Å)	SLD$_h$ (10^{-6}Å^{-2})
0	25	7.5	35.2	50.2	2.03
30	25	7.5	30.5	45.4	3.21
0	50	7.5	30.7	45.7	2.79
30	50	7.5	32.4	47.4	2.99

thickness values. The SLD of the chain region was enforced, as given by eq. (5) and (6). Parameters resulting from the fitting procedure are summarized in Table S3.

The two scattering curves at 50°C are consistent with a spherical 3 shells model (Fig S1 A and B), as are the pure lipid vesicle system at 25°C (Fig S1 C). The SO loaded vesicles at 25°C (Fig S1 D) are much less well described by a spherical shell form factor, as one can see significant deviations from the model in the intermediate regime $2\pi/R_g < q < 2\pi/d_{\mathrm{KP}}$. It suggests that these objects could be either non spherical, or inhomogeneous. We show below that the second hypothesis receive some credentials from the lipid-solvent matching scattering curves.

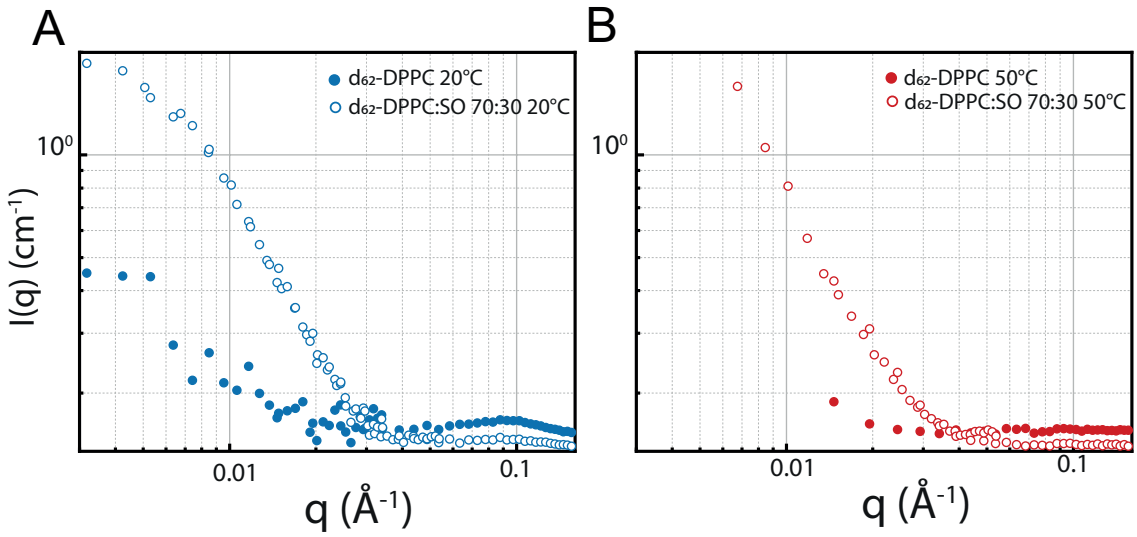

Fig. S5. Small Angle Neutron Scattering (SANS) curves of 50 nm pure d_{62}-DPPC liposome solution and d_{62}-DPPC containing 30% styrene oligomers (SO) in D_2O:H_2O 92:8 recorded below (25°C) and above (50°C) the main phase transition. (A) Comparison of d_{62}-DPPC and d_{62}-DPPC:SO liposomes at 25°C (B) Comparison of d_{62}-DPPC and d_{62}-DPPC:SO liposomes at 50°C. In case of 25°C, the signal arising from lipid only vesicles appears slightly more intense due to changes in the scattering length density of lipids.

B. SANS results under contrast matching conditions. Deuterated lipid d_{62}-DPPC liposomes, which contain fully deuterated hydrophobic chains and hydrogenated headgroup, were prepared in a D_2O:H_2O 92:8 solvent mixture, designed to match the

lipid in the absence of styrene oligomers. As figure S5 indeed shows, the signal in the absence of SO is very weak at both temperatures. As soon as styrene oligomers are added, the scattering intensity rises. The examination of the intensity curve at 25°C hints at a scattering object of gyration radius smaller than the vesicle radius, but larger than the membrane thickness. The scattering intensity at 50°C points to larger objects, although the low q region does not allow for a precise estimation of the gyration radius.

We fitted both curves with a disc model implemented in the SASfit software. The choice of the model was motivated by previous similar analysis of phase separations and disk patches in model membranes (Dao et al (4)). In our case, we fitted the domains with a thin disk form factor, using the *thin disk+homogeneousXS* model of SASfit:

$$|F_{\text{disk}}(q)|^2 = (\pi R^2 L)^2 \left(\eta_{SO} - \eta_{sol}\right)^2 \frac{2}{q^2 R^2} \left(1 - \frac{J_1(2qR)}{qR}\right) \left(\frac{\sin(qL/2)}{qL/2}\right)^2 \quad [9]$$

where L is the disk height, R the disk radius, η_{SO} and η_{sol} the SLD of the styrene oligomers and the solvent, $J_1(x)$ the Bessel function of order 1. The fitted values at 25°C are $R = 350$ Åand $L = 38$ Å. The disk height is compatible with the bilayer thickness. The disc radius is much larger than the bilayer thickness. The scattering curve is therefore consistent with a SO aggregate located in the bilayer vesicle, extended in the transverse direction, but smaller than the vesicle size.

In the case of d_{62}-DPPC:SO liposome at 50°C we decided to employ the same disc model, due to the close overlapping of the two experimental curves in the intermediate region (Fig S5 B), which hints to a similar vertical distribution in the membrane. The scattering curve at 50°C does not reveal a well-defined lateral size, as the Guinier regime is not covered. The value of L was estimated to 34 Å, physically associated to a behavior (eq. 2). The scattering of the SO molecules at high temperature is consistent with polymers inserted into the bilayer, and spreading over larger distances as compared with the low temperature case.

We concluded that our constrast matched scattering experiments support the presence of SO molecules within the lipid bilayer, and that SO is better dispersed in the high temperature fluid phase than in the low temperature gel phase.

Dynamic Light Scattering estimation of the vesicle radius

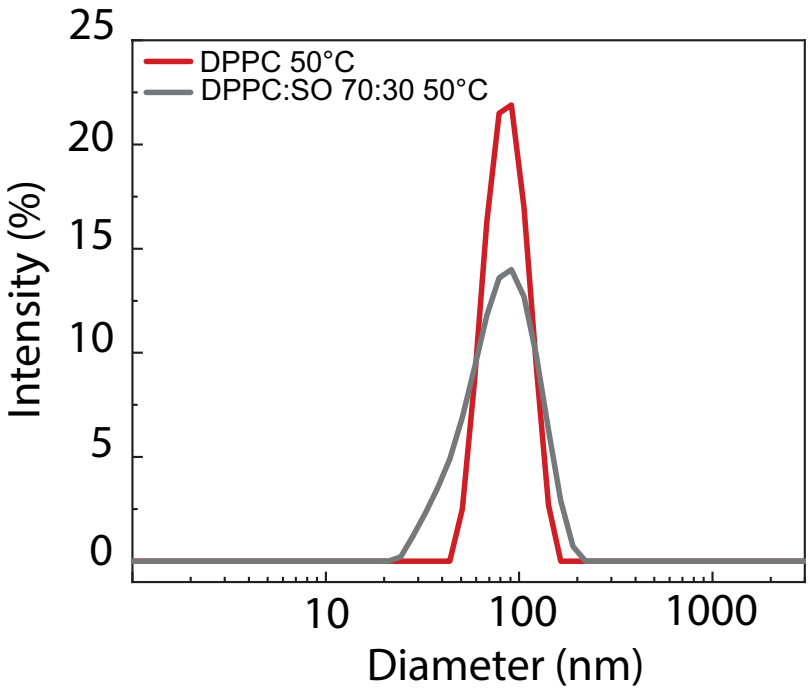

Fig. S6. Size distribution of DPPC and DPPC:SO 100 nm LUVs measured at 50°C. The vesicles show a relatively narrow size distribution. Comparable size between blank and loaded vesicles confirm that SO is present only in vesicles, and not dispersed as mixed DPPC-SO micellar aggregates in solution.

Laurdan emission spectra and Differential Calorimetry Scanning curves

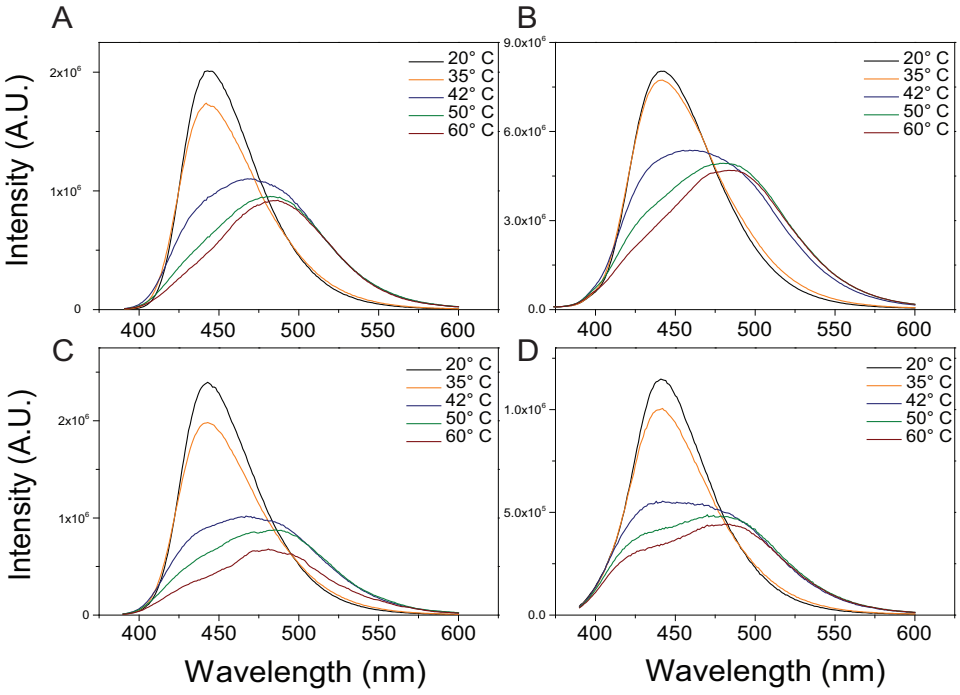

Fig. S7. Comparison of emission curves of Laurdan-labelled 100 nm LUVs for pure DPPC (A), DPPC:SO 90:10 (B), DPPC:SO 80:20 (C) and DPPC:SO 70:30 (D) at 20°C (black line), 35°C (orange line), 42°C(blue line), 50°C(green line) and 60°C (red line).

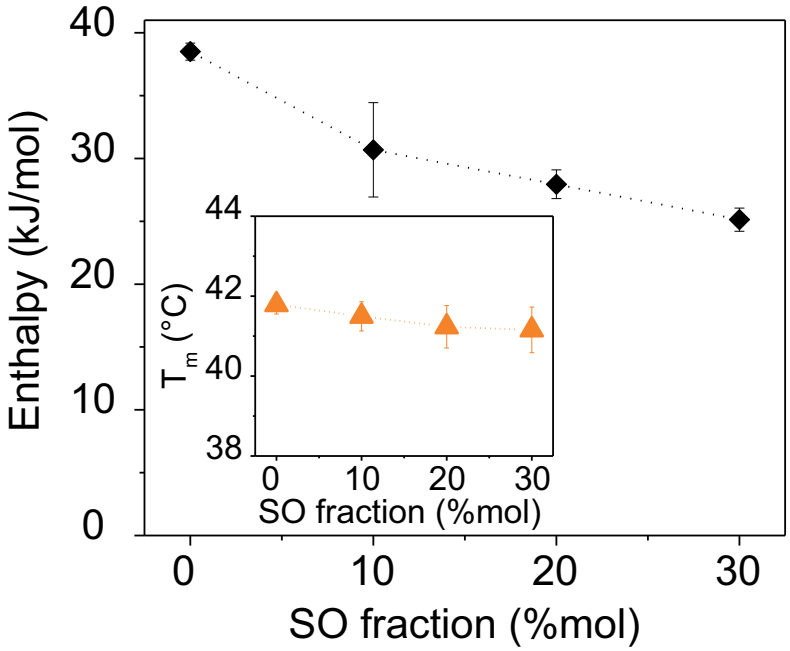

Fig. S8. △H for DPPC 100 nm LUVs containing increasing molar fraction of SO calculated from experimental DSC curves. Inset shows calculated transition temperature T_m at different molar fraction of SO. Each data point and error bars represent the average and standard deviation from two (n = 2) separate samples, with 6 technical repeats each.

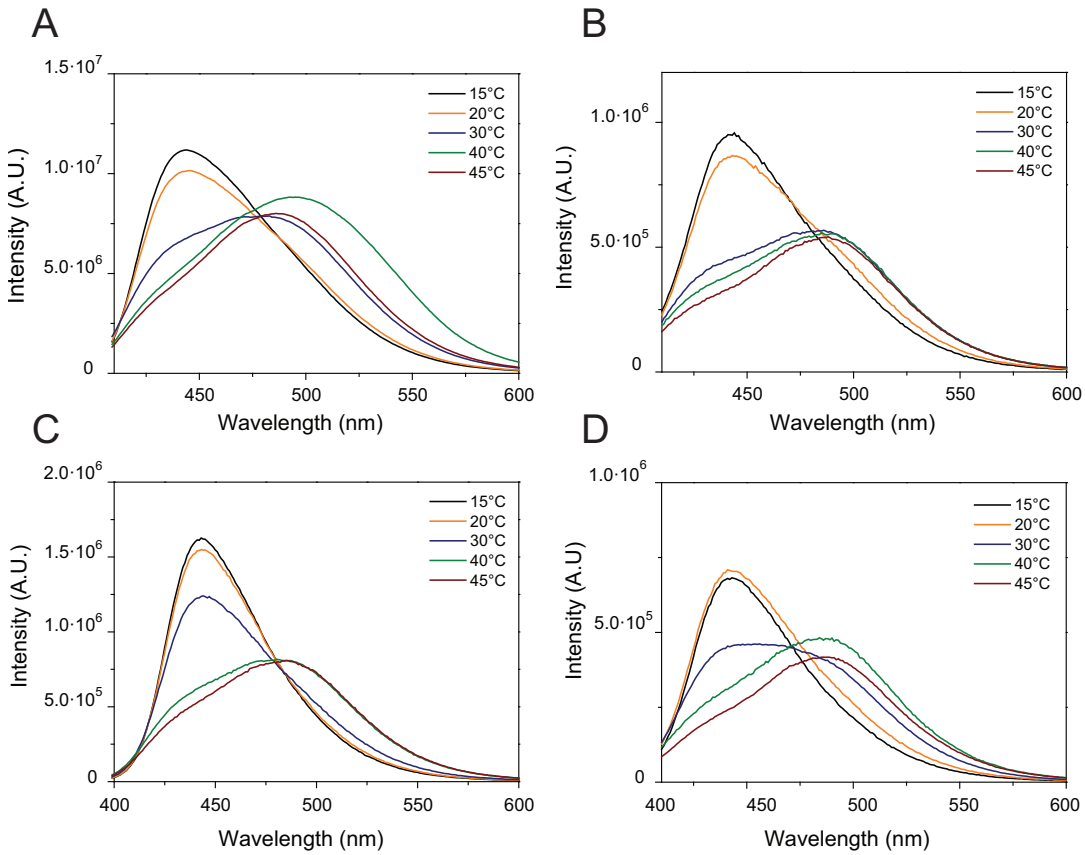

Fig. S9. (A) Comparison of emission curves of Laurdan for DOPC:DPPC 60:40 100 nm LUVs at 15°C (black), 20°C (orange), 30°C (blue), 40°C (green), and 45°C (red). (B) Comparison of emission curves of Laurdan for DOPC:DPPC:SO 54:36:10 100 nm LUVs at 15°C (black), 20°C (orange), 30°C (blue), 40°C (green), and 45°C (red). (C) Comparison of emission curves of Laurdan for DOPC:DPPC 40:60 100 nm LUVs at 15°C (black), 20°C (orange), 30°C (blue), 40°C (green), and 45°C (red). (D) Comparison of emission curves of Laurdan for DOPC:DPPC:SO 36:54:10 100 nm LUVs at 15°C (black), 20°C (orange), 30°C (blue), 40°C (green), and 45°C (red).

Estimation of miscibility temperature from Laurdan GP spectra

To estimate the miscibility temperature between S_o and L_d coexisting phases and a homogenous L_d phase in DOPC:DPPC membranes based on Laurdan GP plots, we have acquired the Laurdan fluorescence spectra at each temperature using excitation wavelengths of 350 nm and 400 nm. As previously described by Parasassi et al. (5), different GP values between excitation at 350 nm and 400 nm will be obtained depending on the phase of the membrane. For a homogenous L_d phase, excitation at 400 nm will yield a lower GP value compared to 350 nm, whereas for coexisting L_d and S_o phases excitation at 400 nm will result in higher GP. Indeed our GP plots (Fig. S10) show this exact trend, as for high temperatures GP values obtained with 400 nm excitation wavelength are significantly lower to 350 nm. The miscibility temperature for each sample was therefore extrapolated by obtaining the temperature at which the two GP curves (350 nm and 400 nm excitation) intersect.

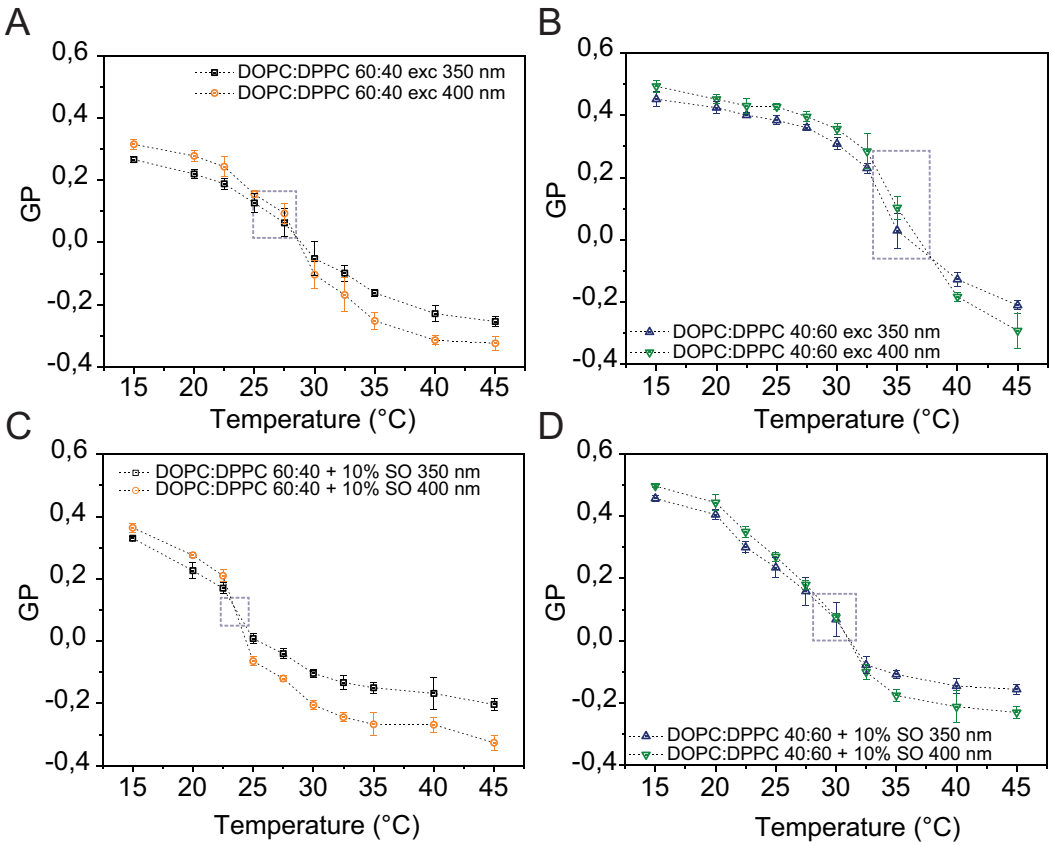

Fig. S10. (A) Variation of general polarization over temperature for 100 nm LUVs of DOPC:DPPC 60:40 excited at 350 nm (black squares) and 400 nm (orange circles). (B) Variation of general polarization over temperature for 100 nm LUVs of DOPC:DPPC:SO 54:36:10 excited at 350 nm (black squares) and 400 nm (orange circles).(C) Variation of general polarization over temperature for 100 nm LUVs of DOPC:DPPC 40:60 excited at 350 nm (blue triangles) and 400 nm (green inverted triangles). (D) Variation of general polarization over temperature for 100 nm LUVs of DOPC:DPPC:SO 36:54:10 excited at 350 nm (blue triangles) and 400 nm (green inverted triangles). Dotted boxes represent the area of confidence for extrapolation of the miscibility temperature. Each data point and error bars represent the average and standard deviation from two (n = 2) separate samples, with 4 technical repeats each for 350 nm excitation wavelength, and 2 technical repeats each for 400 nm excitation wavelength.

Estimation of gel domains area coverage in DOPC:DPPC GUVs

To estimate the area fraction of S_o domains in liquid phase, we analyzed epifluorescence images of giant unilamellar vesicles. the area of solid domain was approximated to a circle of equivalent area. To correct for the sphericity of the vesicles, we tested two different approximations. For both approximations we obtained similar values of area coverage. In case of vesicles presenting multiple domains or very elongated domains we subdivided the area covered by the solid phase into smaller approximated circles.

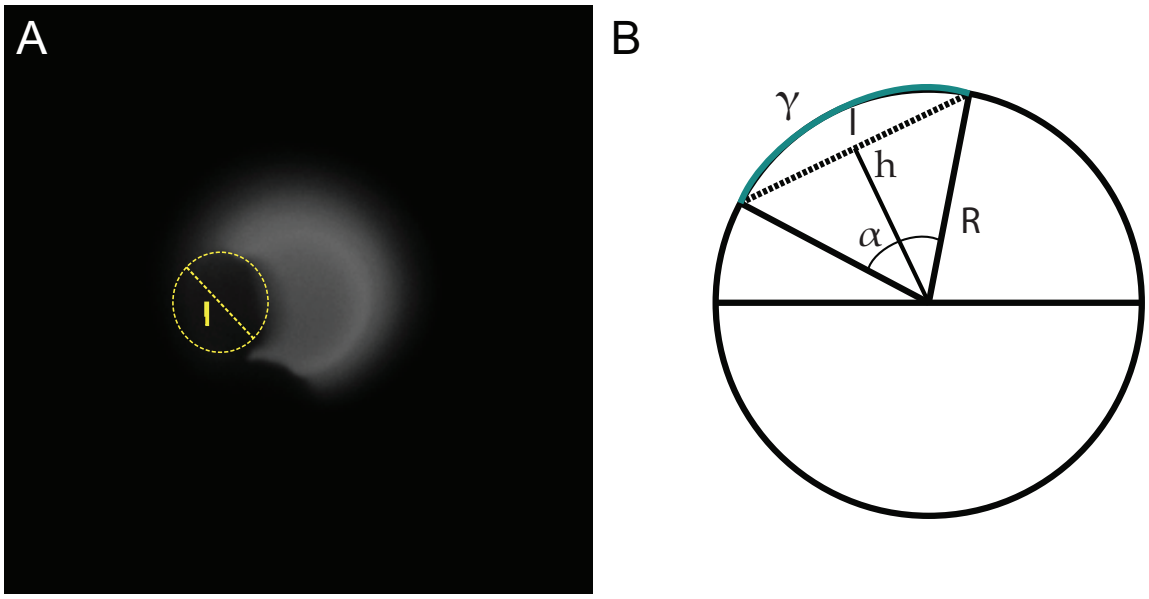

Fig. S11. Principle of measurement of the fraction of the ordered phase from a giant vesicle. A) Typical image and domain detection. B) Geometric representation of the relevant lengths and angles.

The area of the domain can be obtained by the measured diameter l (Fig S11 A), which must be corrected to account for the curvature of the GUV. To determine the real length of the domain, it is necessary to calculate the arc length γ spanned by a projected length l. Using a circular approximation (Fig S11 B) yields that the arc length γ is equal to:

$$\gamma = \frac{\alpha}{\pi} \cdot 2\pi R \qquad [10]$$

where α is the angle in radians spanned by the length l. The angle α can be calculated by considering that

$$\frac{\alpha}{2} = \arccos(\frac{h}{R}) \qquad [11]$$

where $h = \sqrt{R^2 - (l/2)^2}$ is the distance from the center of the projected l to the center of the circle. The fraction f_b of the solid area with respect to the area of the vesicle is defined as:

$$f_b = \frac{S_g}{S_{GUV}} = \frac{2\pi(\gamma/2)^2}{4\pi R^2} = \frac{\gamma^2}{8R^2} \qquad [12]$$

Therefore combining equation 12, 10 and 11, we obtain

$$f_b = \frac{1}{2R} \cdot \arccos(\frac{\sqrt{R^2 - (l/2)^2}}{R}) \qquad [13]$$

In the case when GUVs with individual hexagonal domains are not present or closely neighboring each other, giving rise to a complex domain such as in the Fig S12 A, the circular approximation of the domains was maintained, but the domain was segmented into small circles to encompass the domain area as shown in Fig S12 B. The overall area of the circles was then used to extrapolate an equivalent domain radius, and then utilized to calculate the area coverage as explained before.

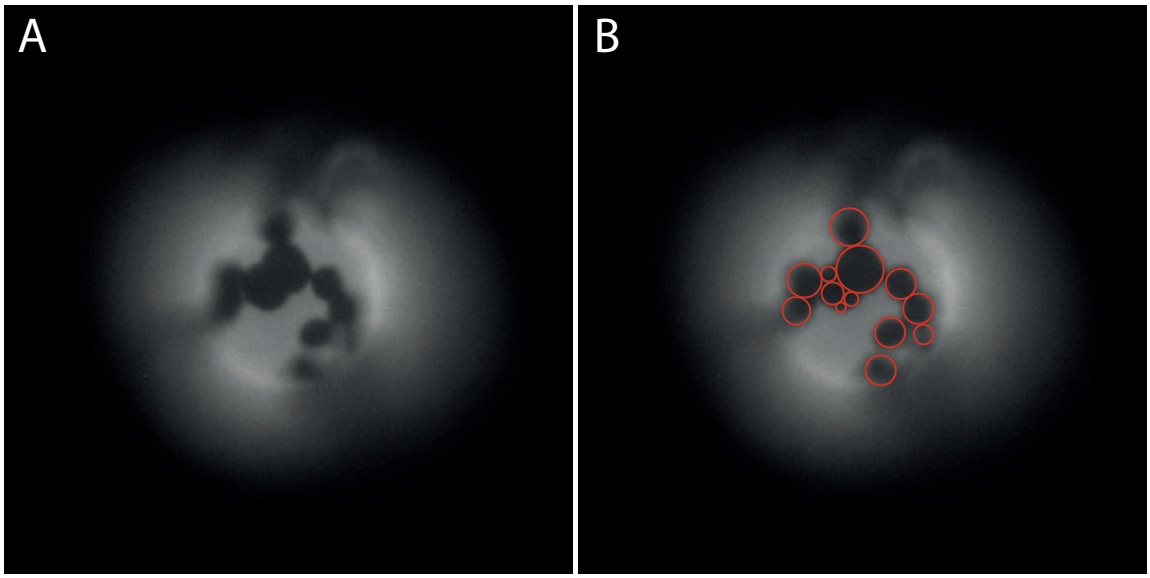

Fig. S12. A) GUV displaying a complex domain morphology. B) Example of manual tessellation performed to measuree S_o domains area coverage in GUVs with such complex domain morphology.

References

1. J Pencer, FR Hallett, Small-angle neutron scattering from large unilamellar vesicles: An improved method for membrane thickness determination. *Phys. Rev. E* **61**, 3003–3008 (2000).
2. R Sreij, et al., Dmpc vesicle structure and dynamics in the presence of low amounts of the saponin aescin. *Phys. Chem. Chem. Phys.* **20**, 9070–9083 (2018).
3. J E. Mark, et al., *Physical Properties of Polymers*. (2004).
4. TPT Dao, et al., Phase separation and nanodomain formation in hybrid polymer/lipid vesicles. *ACS Macro Lett.* **4**, 182–186 (2015).
5. T Parasassi, G De Stasio, G Ravagnan, R Rusch, E Gratton, Quantitation of lipid phases in phospholipid vesicles by the generalized polarization of laurdan fluorescence. *Biophys. J.* **60**, 179 – 189 (1991).